Chemical Engineering Journal 469 (2023) 143713

Contents lists available at ScienceDirect

Chemical Engineering Journal

journal homepage: www.elsevier.com/locate/cej

Optimal experimental design for the identification of a reaction kinetic model for the hydroaminomethylation of 1-decene in a thermomorphic multiphase system

Karsten H.G. Rätze [a], Wieland Kortuz [b], Sabine Kirschtowski [b], Michael Jokiel [c], Christof Hamel [b], Kai Sundmacher [a,c,*]

[a] Otto von Guericke University Magdeburg, Chair for Process Systems Engineering, Universitätsplatz 2, D-39106 Magdeburg, Germany
[b] Otto von Guericke University Magdeburg, Chair of Chemical Process Engineering, Universitätsplatz 2, D-39106 Magdeburg, Germany
[c] Max Planck Institute for Dynamics of Complex Technical Systems, Department Process Systems Engineering, Sandtorstr. 1, D-39106 Magdeburg, Germany

ARTICLE INFO

Keywords:
Transient multiphase systems
Model-based optimal experimental design
Mechanistic kinetics
Parameter estimation
Hydroaminomethylation
Dynamic optimization

ABSTRACT

The transition toward green chemicals production requires new processes which are able to handle sustainable feedstock comprising unsaturated, long-chain hydrocarbons. The homogeneously rhodium-catalyzed tandem hydroaminomethylation (HAM) is able to convert long-chain olefins to amines and, therefore, represents an example reaction of high interest for the next generation of chemical processes. This work improves upon an existing mechanistic reaction kinetic model for 1-decene in a methanol/dodecane thermomorphic multiphase system (TMS) by structural adjustment of the catalyst pre-equilibrium, the investigation of the water influence on the reaction equilibria as well as the re-estimation of kinetic and inhibition parameters to provide accurate predictions under a wide range of operating conditions. This is achieved by pairing model-based optimal experimental design (mbOED) with perturbed-chain statistical associating fluid theory (PC-SAFT)-based phase equilibrium calculations to account for experiment setup-specific limitations while ensuring monophasic operation throughout all experiments. The subsequent model identification is able to substantially improve the prediction quality of the hydroaminomethylation model in edge cases over the previous model while maintaining a quantitative agreement of experimental and simulated concentration profiles under nominal conditions.

1. Motivation

Aliphatic amines are essential for the production of agrochemicals, surfactants, herbicides and pharmaceuticals [1,2]. From the total annual production capacity of 1.9×10^6 ta^{-1} in 2013 [1], the majority of amines produced fall in the category of linear amines in contrast to their branched counterparts due to their utilization as intermediates in the bulk chemicals production [3]. Depending on the alkyl chain length, amines with a short chain length can be produced in gas phase while long-chain amines require liquid phase processes with polar and/or non-polar solvents. These solvents are required to facilitate the reaction and enable catalyst recovery in the case of homogeneous catalysis. In the face of the sustainable transformation of the chemical industry which will increase the demand for biomass-based raw materials, substrates with long alkyl chains will substitute today's short-chain, fossil-based feeds [4]. Therefore, new reactions and processes need to be invented which are able to meet the new requirements to facilitate an efficient and selective chemicals production.

Hydroaminomethylation. The homogeneously rhodium-catalyzed autotandem hydroaminomethylation (HAM) represents such a reaction as it is able to produce linear amines from long-chain olefins in liquid phase using bidentate phosphine ligands for increased selectivity [5–7]. This one-pot synthesis is a combination of the hydroformylation (Hyfo) and reductive amination (RA) where the long-chain olefin is first converted to a linear aldehyde using syngas (CO and H_2). In the

* Corresponding author at: Max Planck Institute for Dynamics of Complex Technical Systems, Department Process Systems Engineering, Sandtorstr. 1, D-39106 Magdeburg, Germany.
E-mail addresses: raetze@mpi-magdeburg.mpg.de (K.H.G. Rätze), wieland.kortuz@ovgu.de (W. Kortuz), sabine.kirschtowski@ovgu.de (S. Kirschtowski), jokiel@mpi-magdeburg.mpg.de (M. Jokiel), christof.hamel@ovgu.de (C. Hamel), sundmacher@mpi-magdeburg.mpg.de (K. Sundmacher).

https://doi.org/10.1016/j.cej.2023.143713
Received 21 March 2023; Received in revised form 19 May 2023; Accepted 21 May 2023
Available online 25 May 2023

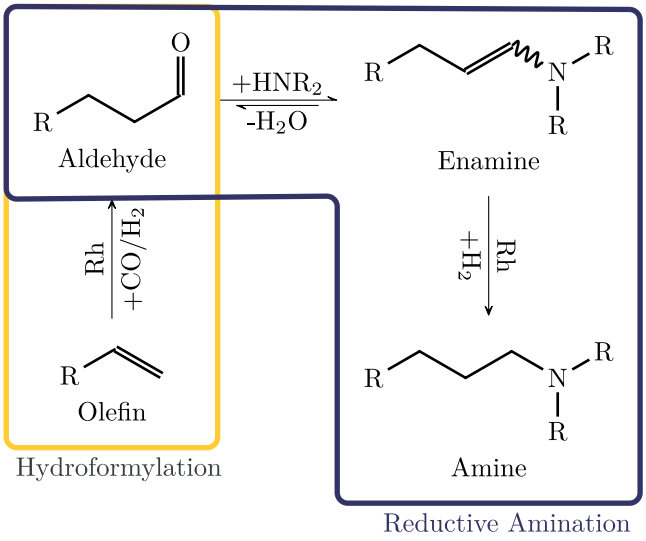

Fig. 1. General HAM reaction sequence for a linear olefin [8].

presence of an amine as co-substrate, the linear aldehyde reacts in an equilibrium-limited condensation reaction under water release to the enamine/imin from which the final amine is formed via hydrogenation. A schematic representation of the main reaction pathway is depicted in Fig. 1.

Solvent system. For an economic process operation, efficient recycling of the rhodium catalyst is mandatory [9]. Besides other alternatives, this can be achieved using a thermomorphic multiphase system (TMS) which comprises a polar and non-polar solvent with a temperature-dependent miscibility gap [10]. Utilization of such a solvent system allows the monophasic operation at reaction temperature while the recovery of the polar catalyst is facilitated via the polar phase after initiating a phase split at reduced temperatures. If the distribution coefficient of the catalyst between both phases is not sufficient for an economic operation, employment of a counter current decanter cascade improves the separation results and enables the separation at ambient temperatures [9].

Experimental challenges. Depending on the operating conditions, the accumulation of water in combination with the TMS can lead to the formation of a water-rich, second phase at reaction temperature. Besides the introduction of mass transfer resistances, the polar catalyst is drawn to this aqueous phase which impedes the reaction progress. This decrease of the available catalyst in the reaction phase needs to be prevented for the identification and parameterization of a reaction kinetic model so that carefully designed experiments are mandatory. To account for the complex temperature and species concentration dependency of the miscibility gap, model-based optimal experimental design (mbOED) methods are employed. In addition to the previously mentioned advantages, these methods are particularly suited for the HAM as constraints can be introduced which ensure the monophasic state of the system. Therefore, this contribution proposes the combination of rigorous phase equilibrium calculations based on the state-of-the-art perturbed-chain statistical associating fluid theory (PC-SAFT) equation of state (EoS) with the simultaneous model-based design of multiple experiments to identify operating conditions of maximum information content. These designs are implemented in lab-scale experiments after which the results are used to formulate as well as calibrate a reactor vessel and reaction kinetic model for the HAM of 1-decene.

Scope of this contribution. After the introduction of the kinetic model for the HAM, the mbOED formulation strategy is outlined and the calculated experiment designs are presented. Based on these designs, experiments were performed which are used to refine the gas phase description of the reactor vessel model, introduce modifications to the catalyst pre-equilibrium formulation, and calculate new kinetic parameter estimates. The prediction results using the original and improved model formulation are compared before the article closes with a results summary and concluding remarks.

2. Kinetic model

The HAM reaction network contains a variety of reactions such as the olefin isomerization, the olefin, aldehyde and enamine hydrogenation, the Hyfo as well as the aldol and enamine condensation. An overview over the reaction network is depicted in Fig. 2.

Due to the formation of branched aldehydes in the Hyfo, branched amines are potential products of the HAM as well.

Catalyst pre-equilibrium. To ensure a regioselective production of linear amines, catalyst ligands are required for a favorable n/iso ratio. From the group of bidentate phosphine ligands, SulfoXantphos is chosen because of its water tolerance in combination with its appropriate polarity for separation and recoverability using a methanol (MeOH)/n-dodecane (nC12an) TMS [12]. The catalyst precursor Rh(acac)(COD) is similar to the one used for the Hyfo model from Jörke et al. [13] (Rh(acac)(CO_2)) and is assumed to follow the same catalyst cycle with a resting and active state. With the additional assumption of only one prevailing active catalyst species which is catalyzing each of the catalyzed reactions in the HAM, the catalyst pre-equilibrium

$$c_{\mathrm{cat}} = \frac{c_{\Sigma\mathrm{cat}}}{1 + K_{\mathrm{cat,CO}} c_{\mathrm{CO}}}, \tag{1}$$

is adopted. In this pre-equilibrium, an excess of carbon monoxide (CO) limits the formation of the active catalyst species from the total amount of catalyst precursor $c_{\Sigma\mathrm{cat}}$ provided.

Mechanistic model structure. To ensure the identifiability of all reaction kinetic parameters under consideration of a limited number of experiments, the kinetic network from Fig. 2 needs to be reduced to a set of reactions which capture the essential system behavior under a variety of operating conditions.

Kortuz et al. [6] proposed a mechanistic kinetic model for the tandem HAM reaction of 1-decene in a MeOH/nC12an TMS by combining the kinetic models of Jörke et al. [13] and Kirschtowski et al. [7] for the underlying Hyfo of 1-decene and RA of 1-undecanal, respectively. It is important to note that the RA system of Kirschtowski et al. [7] differs from the Hyfo system of Jörke et al. [13] in terms of the TMS, catalyst precursor and ligand. Therefore, Kortuz et al. [6] not only formulated the kinetic structure based on those prior contributions but also executed an heuristic set of experiments for the reparameterization to correct any inaccurate predictions. In a recent contribution, Kortuz et al. [15] extended the reparameterized model by a mechanistic formulation of the final hydrogenation step, allowing a fully mechanistic description. The experiments in both contributions were primarily focused on the temperature, pressure and solvent system effects. This work aims at refining the kinetic model further by systematically considering a variety of influences, such as the gas phase composition and, in particular, the impact of water on the reaction progress. Therefore, the kinetic network and reaction rate equations of Kortuz et al. [15] are used as an initial guess during mbOED. A schematic representation of this network is depicted in Fig. 3.

Reaction rate definition. In the first step, the α-olefin 1-decene is converted in the Hyfo r_{Hyfo} to the linear aldehyde 1-undecanal (nC11al). This intermediate product reacts in an equilibrium reaction with the co-substrate diethylamine (DEA) in the enamine condensation r_{Cond} under the release of water to the enamine, n,n-diethylundecylamine (enamine). In the last step, the enamine is hydrogenated r_{HydEn} to the final amine, n,n-diethylundecylamine (hydrogenated) (amine). In addition to this primary reaction pathway, the olefin isomerization r_{Iso} to a lumped

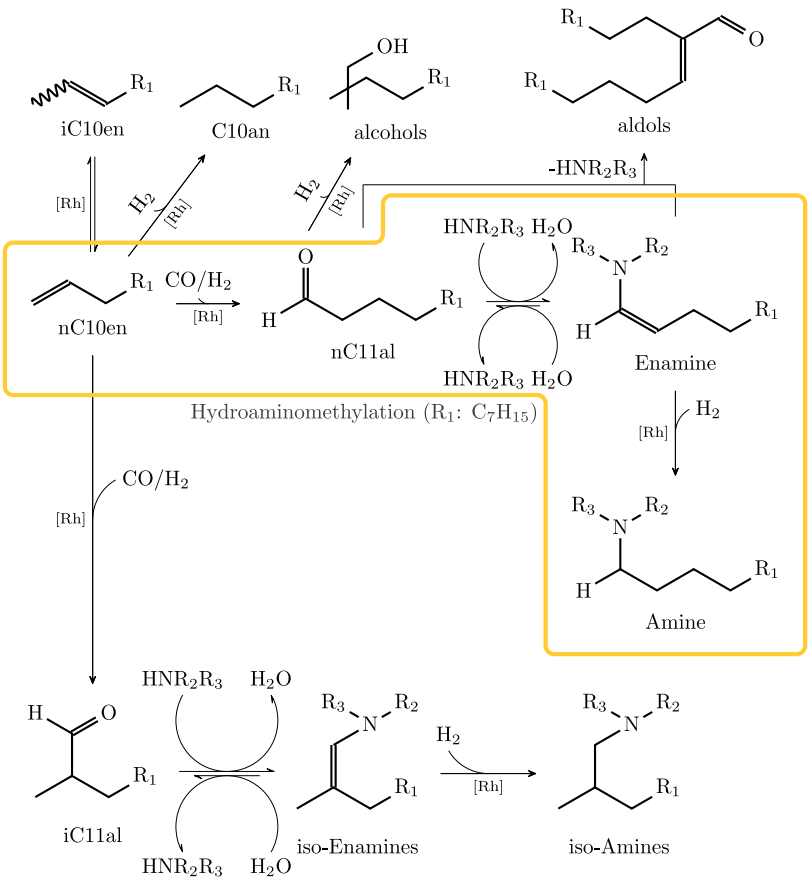

Fig. 2. Detailed reaction network of the rhodium-catalyzed HAM with side reactions.
Source: Adopted from [11].

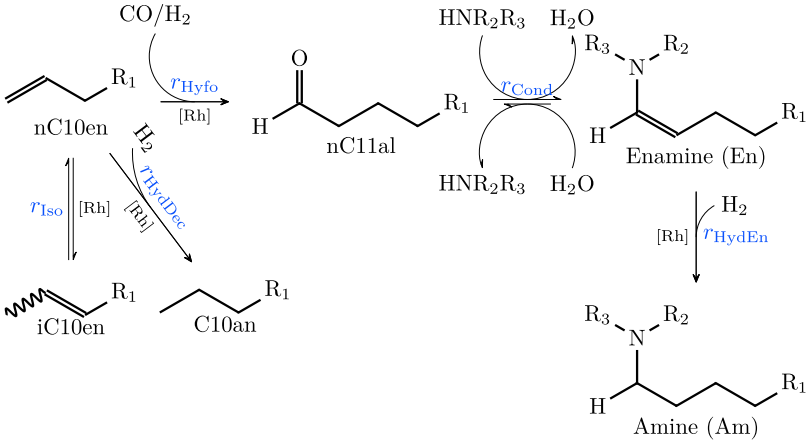

Fig. 3. Reduced reaction network of the HAM of 1-decene in a MeOH/nC12an TMS.
Source: Adopted from [6,14].

species iC10en [16,17] as well as the olefin hydrogenation r_{HydDec} are considered. While the influence of the latter reaction is non-negligible due to significant decane concentrations in preliminary experiments under nominal operating conditions, the isomerization reaction is incorporated preliminary due to its inhibiting effect on the main reactions in the edge cases of low syngas concentrations. In contrast to the rate formulation from Kortuz et al. [15] which is based on Jörke et al. [18], the isomerization kinetic model is chosen according to Hyfo reaction kinetics from Jörke et al. [13] to limit the number of parameters during mbOED as well as parameter estimation. Other side reactions, such as the aldol condensation, the Hyfo to branched aldehydes and the aldehyde hydrogenation, are not considered. Thus, the reaction rates can be summarized in the set $\mathcal{RCT}^{HAM}$ = {Hyfo, Iso, HydDec, Cond, HydEn} with the reaction rate expressions

$$r_{Iso} = k_{Iso} c_{cat} \left(c_{nC10en} - \frac{c_{iC10en}}{K_{Iso}^{eq}} \right), \tag{2a}$$

$$r_{Hyfo} = \frac{k_{Hyfo} c_{cat} c_{nC10en} c_{H_2} c_{CO}}{1 + K_{Hyfo,I} c_{H_2} + K_{Hyfo,II} c_{H_2} c_{CO}}, \tag{2b}$$

$$r_{\mathrm{HydDec}} = \frac{k_{\mathrm{HydDec}} c_{\mathrm{cat}} c_{\mathrm{nC10en}} c_{\mathrm{H_2}}}{1 + K_{\mathrm{HydDec}} c_{\mathrm{H_2}}}, \tag{2c}$$

$$r_{\mathrm{Cond}} = k_{\mathrm{Cond}} \left(c_{\mathrm{nC11al}} c_{\mathrm{DEA}} - \frac{c_{\mathrm{En}} c_{\mathrm{H_2O}}}{K^{\mathrm{eq}}_{\mathrm{Cond}}(T)} \right), \tag{2d}$$

$$r_{\mathrm{HydEn}} = \frac{k_{\mathrm{HydEn}} c_{\mathrm{cat}} c_{\mathrm{En}} c_{\mathrm{H_2}}}{1 + K_{\mathrm{HydEn}} c_{\mathrm{H_2}}}. \tag{2e}$$

For each reaction $j \in \mathcal{RCT}^{\mathrm{HAM}}$, the kinetic factor

$$k_j(T) = \exp\left(A_j + B_j \frac{T - T_{\mathrm{ref}}}{T} \right), \tag{3}$$

follows the Arrhenius approach with the dimensionless parameters A_j and B_j. These dimensionless parameters relate to the collision factor $k_{0,j}$ and activation energy $E_{\mathrm{A},j}$ according to

$$k_{0,j} = \exp\left(A_j + B_j \right), \tag{4a}$$

$$E_{\mathrm{A},j} = B_j R T_{\mathrm{ref}}, \tag{4b}$$

with $T_{\mathrm{ref}} = 373.15\,\mathrm{K}$ [19]. The temperature-dependent condensation equilibrium constant

$$K^{\mathrm{eq}}_{\mathrm{Cond}}(T) = \exp\left(\frac{-\Delta G_{\mathrm{r,Cond}}}{RT} \right), \tag{5}$$

is taken from Kirschtowski et al. [7] without modification because of extensive experimental and simulative investigations in a matching reaction system. In contrast, the isomerization equilibrium constant $K^{\mathrm{eq}}_{\mathrm{Iso}}$ cannot be taken from Jörke et al. [13] due to the utilization of a different solvent system. Therefore, preliminary equilibrium experiments are used to identify the equilibrium constant to $K^{\mathrm{eq}}_{\mathrm{Iso}} = 39.0$ (see table S1 and Fig. S1 in the supplementary material for the experimental data and a comparison to the parameter values from Jörke et al. [13]). Because of the promising results from Kortuz et al. [15], the inhibition constants for the Hyfo as well as decene and enamine hydrogenation reactions are considered constant during parameter estimation.

3. Model-based optimal experimental design

mbOED design decision. For the refinement of the HAM model, five experiments are designed using the parallel approach in mbOED [20]. In contrast to the sequential design which is frequently encountered in the literature, the simultaneous design allows for the concurrent consideration of all available degrees of freedom (DoFs). Consequently, the experiments can be designed to optimally complement each other while also preventing identical designs as trivial solutions [20]. Finally, this approach can be extended by sequentially designing multiple experiments according to the hybrid approach proposed by Barz et al. [21]. Downsides of the simultaneous design include the large design space, a multitude of local optima and numerical difficulties due to the problem size. In this work, these downsides can be circumvented by the limited number of experiments in addition to reliable initial guesses in terms of the kinetic model structure and parameters from Kortuz et al. [15].

Monophasic requirement. The formation of water as a by-product in the enamine condensation may lead to the occurrence of multiple liquid phases due to the limited water tolerance of the MeOH/nC12an TMS [22]. For the accurate determination of reaction kinetics, this phase split needs to be prevented as additional transport resistances and the accumulation of the polar catalyst in the aqueous phase leads to biased parameter estimates. Box constraints on the operating window can be used to prevent unfavorable operating conditions but significantly reduce the experiment design space. By incorporating rigorous phase equilibrium calculations in the mbOED problem, monophasic reaction conditions are ensured while simultaneously exploiting a maximally large feasible region.

Phase equilibrium calculation. Rigorous phase equilibrium calculations require fugacity/activity coefficient models to capture the non-ideality of species mixtures. For the HAM, utilization of the PC-SAFT EoS for the activity coefficient calculation is beneficial because of accurate predictions as shown by Huxoll et al. [23]. Instead of direct utilization of the PC-SAFT model, an artificial neural network (ANN) for the intended operating window is created due to numeric and performance concerns. For details on the ANN training and comparison to modified UNIFAC(Dortmund) (modUNIFAC), the interested reader is referred to Supplement D. Combined with the dynamic method for phase equilibrium calculations by Zinser et al. [24] (see Supplement C), the rigorous calculation of the system state can be performed during mbOED and enables the restriction to monophasic operation. The significant computational load introduced by the rigorous phase equilibrium calculations is restricted by focusing on the calculation at the final time t^{f}_k of each experiment $k \in \mathcal{EXP}$. Despite this restriction, the design decision does not lead to inaccuracies in the results as water is accumulated over time while the thermostat of the experimental setup does not allow for active cooling. Hence, the final time of each experiment serves as a good indicator for multiphasic behavior since no phase union is possible in the considered operating window (see table S10).

Decision variables. With the special focus on practicability of the experimental designs, the reaction rates from Eq. (2) are embedded in a reactor vessel model where the temperature T, pressure p and gas phase compositions y_{CO}, $y_{\mathrm{H_2}}$, $y_{\mathrm{N_2}}$ are considered as states rather than controls. Instead, their derivatives with respect to (w.r.t.) time are added as alternative controls which allows for the precise incorporation of thermostat heating/cooling rates, valve specifications and experimental limitations. Please note that nitrogen serves as an inert component providing additional DoF during mbOED. Besides these time-dependent control variables, the experiment time t^{f}, the co-substrate to substrate ratio $\phi^{\mathrm{n,0}}_{\mathrm{DEA,sub}}$ and the initial water amount $\phi^{\mathrm{V,0}}_{\mathrm{H_2O}}$ are considered as control parameters. For the ratio definitions, please consult Eq. (B.5) in Supplement B.1. Additionally, the mbOED problem is formulated with restrictions on the minimum interval between two successive, optimal measurement times to ensure the feasibility of the experiment. For detailed information on the reactor vessel model and the mbOED problem formulation, the interested reader is referred to Supplement B and Supplement E, respectively.

Uncertain parameter selection. With the goal of refining the kinetic parameters from Kortuz et al. [15], the mbOED is designed to focus on the dimensionless parameters A_j and B_j with $j \in \mathcal{RCT}^{\mathrm{HAM}}$. For five reaction rates, this would result in ten parameters for which the sensitivity equations need to be solved. Together with eight measurable species (see Eq. (B.3) in Supplement B.1) and the simultaneous design of five experiments, this optimization requires excessive computational power. Without the utilization of surrogate models or compromises w.r.t. the number of measured species and designed experiments, complexity reduction potential can be found in the parameter selection. In a first step, the 1-decene hydrogenation can be neglected as it is not part of the main reaction pathway and does not lead to a subsequent reaction network. Hence, A_{HydDec} and B_{HydDec} are removed from the set of uncertain parameters in the mbOED. Additionally, the strong similarity of the variational equations w.r.t. A and B (see Supplement G) allow for a significant reduction of computational load with only minimal approximation errors. Therefore, the uncertain parameter vector θ is limited to the dimensionless activation energies B_j with $j \in \{\mathrm{Iso}, \mathrm{Hyfo}, \mathrm{Cond}, \mathrm{HydEn}\}$.

4. Experiment design for the hydroaminomethylation of 1-decene

The computational complexity of the mbOED problem limits the number of experiments which can be designed simultaneously. This restriction is tolerable because of the already determined first parameters in the previous work form Kortuz et al. [15] so that $n_{\mathrm{exp}} = 5$ represents

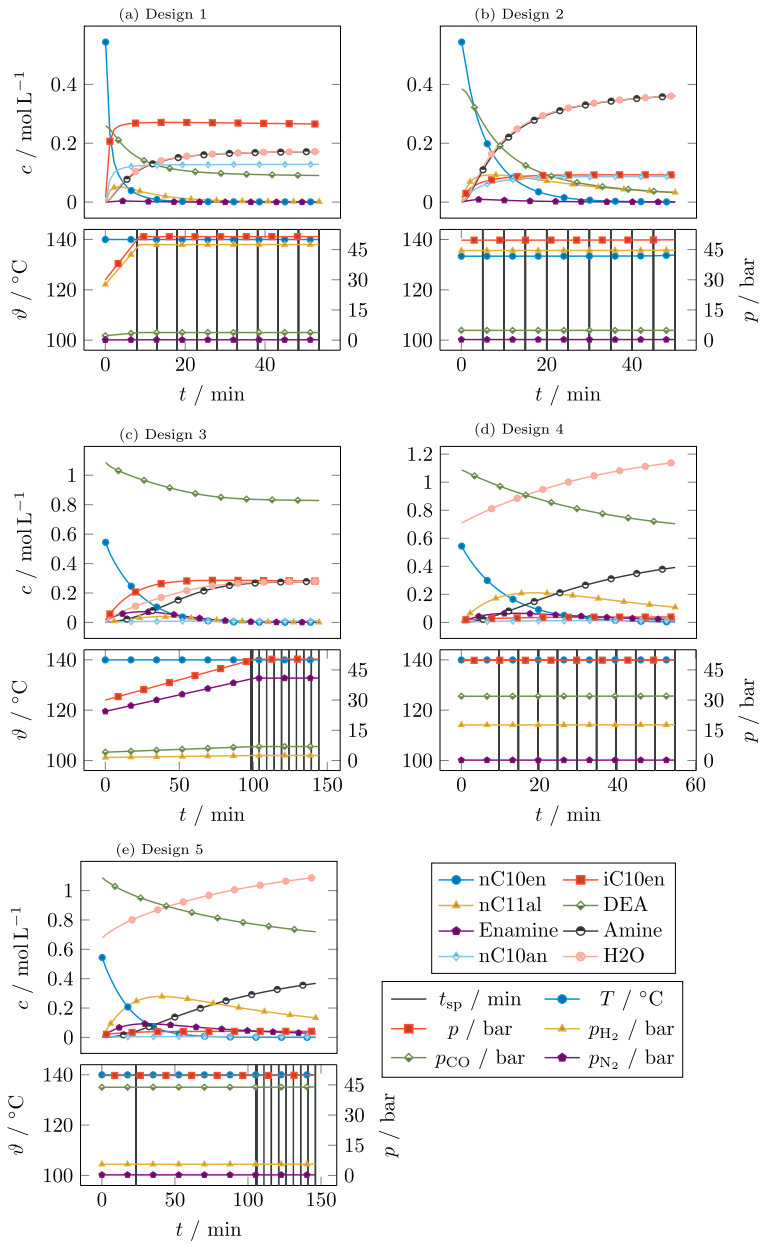

Fig. 4. D-optimal concentration and control trajectories resulting from the simultaneous mbOED solution of Eq. (E.6) with $n_{exp} = 5$. The vertical lines in the control profile plots represent the optimal measurement points. The corresponding optimal control parameters p^* can be found in Table 1.

a compromise between information gain and problem feasibility. As objective function, a D-optimal design is selected which enables minimization of parameter uncertainty and parameter correlations while avoiding excessive computational loads of more sophisticated multi-criteria and eigenvalue- or singular-value-based criteria designs. Implementational details on the mbOED problem formulation as well as the initialization strategy can be found in Supplement E.

4.1. Results

The designs for all five experiments are depicted in Fig. 4 and show the concentration and control profiles. The corresponding optimal control parameters are summarized in Table 1.

In all cases, the solver is able to identify a unique set of experiment designs which focus on different aspects of the reaction system. While the first design emphasizes the isomerization reaction, the second and third design use different initial DEA concentrations and gas phase ratios to investigate the influence on the main reaction pathway. The last two designs utilize an initial water content to shift the enamine condensation equilibrium and provide kinetic information for the intermediate products. Despite similar concentration profiles, designs 4 and 5 differ in terms of their time horizon.

Table 1
Optimal control parameters for the D-optimal, simultaneous mbOED solution of Eq. (E.6) with $n_{exp} = 5$.

Design	1	2	3	4	5
t^f / min	54	50	144	55	146
$\phi^{n,0}_{DEA,sub}$ / mol mol^{-1}	0.48	0.71	2.00	2.00	2.00
$\phi^{V,0}_{H_2O}$ / L L^{-1}	0.00	0.00	0.00	0.014	0.0134
y_{H_2} / mol mol^{-1}	0.92	0.90	0.05	0.35	0.11
y_{CO} / mol mol^{-1}	0.07	0.10	0.14	0.64	0.88

Control profile analysis. When focusing on the control profiles as illustrated in Fig. 4, it becomes clear that the different characteristics of the concentration profiles primarily stem from the initial concentrations and control parameters in contrast to the temperature and partial pressure profiles. While the temperature remains constant in all experiments, the only instances of control profile formation can be found in designs 1 and 3. In the former case, the first 10 min are used to elevate the total pressure from 30 bar to the upper bound of 50 bar by increasing the hydrogen (H_2) content in the gas phase. This leads to a rising concentration of the hydrogenation product and moderate levels of amine formation due to reduced Hyfo activities. In the latter case, the pressure increase is prolonged over a 100 min period in which the nitrogen content grows significantly. Serving as an inert component, the nitrogen does not have a direct effect on the reaction kinetics. However, the solver chooses to utilize the nitrogen as a diluting agent for the gas phase as it allows partial pressures for H_2 and CO which cannot be attained via the manipulation of the total pressure because of its lower bound at 30 bar (see table S10).

In terms of the temperature profiles, the solver does not try to include a temperature ramp in the experiment designs as temperature variations are normally favorable for the identification of the (dimensionless) activation energy. While maintaining a maximum temperature of 140 °C in designs 4 and 5 appears reasonable to prevent phase separation under elevated water concentrations, designs 1 to 3 do not seem to be directly affected by this restriction. Possible explanation include (i) the minor effect of a temperature profile which is bound by a maximum slope of 2.5 K, (ii) the comparatively low DEA content in designs 1 and 2 which limits the water tolerance of the TMS, especially at low temperatures, (iii) the sharp increase in isomer concentration for design 1 requiring high temperatures, (iv) reduced reaction rates in design 3 which require maximum temperatures to achieve the desired conversion level and (v) the identification of a local optimum despite the initialization strategy from Supplement E.2.

Measurement time discussion. For each experiment, 10 optimal measurement points are identified by the solver. These measurement points are constrained in terms of the time horizon from 50 min to 180 min and via a minimum distance between two consecutive measurements of 5 min (see Eq. (E.6) and table S10). Regarding the experiment designs in Fig. 4 and Table 1, a wide range of experiment durations from 50 min to 146 min is utilized. By reducing the time horizon and the measurement intervals to their respective lower bound, the solver is able to achieve a higher sampling frequency in designs which focus on intermediate products as well as high reaction rates and elevated product yields (see Figs. 4(a), 4(b) and 4(d)). Alternatively, the time horizon is expanded to yield repetitive measurements during steady-state (see Fig. 4(c)) or increase the information gain by complementing other experiments which may not be continued due to critical water concentrations and the risk of phase separation (compare Figs. 4(d) and 4(e)).

4.2. Design discussion

Seeking a quantitative assessment of the experiment designs in Fig. 4, Table 2 contains simple uncertainty measures such as the uncertainty ellipsoid volume, parameter standard deviation and correlation coefficients for each design. While the reference uncertainty measures for the combination of all five experiments is shown at the top, relative values are calculated for the designs by removing experiment k from the set $\mathcal{EXP}$ before recalculating the uncertainty measures and comparing the results to the reference. Relying on a relative comparison of the uncertainty measures ensures that the negative impact of a reduced number of experiments on the information content is mediated. This enables the analysis of the relative impact of each design on the overall and specific parameter uncertainty and, by virtue of the selected uncertain parameters, the primary association of each design to a reaction.

When focusing on designs 1 to 3, the strong positive impact on the uncertainty ellipsoid volume can be explained by two factors. If removed from the experiment set, each of the designs causes a significant increase of the standard deviation of one of the reactions. While design 1 seems to primarily contain information on the Hyfo, the enamine condensation and decene isomerization are sensitive to the operating conditions of design 2 and 3, respectively. As a second factor, all three designs positively impact the parameter correlations with regard to at least one parameter pair. For design 1, the decorrelating effect is particularly pronounced for the isomerization and Hyfo, Hyfo and enamine condensation, as well as isomerization and enamine hydrogenation reactions. A similar effect on the Hyfo and enamine condensation reaction is present for design 2 while design 3 reduces correlations between the isomerization and Hyfo in addition to the isomerization and enamine hydrogenation reactions. Due to the complex impact of each design on the uncertainty measures of the experiment set, designs 1 and 3 also introduce parameter correlations for the enamine condensation and enamine hydrogenation. This adverse effect is indicated by the negative values in the correlation matrix column in Table 2.

In contrast to the first three designs, designs 4 and 5 have a negligible or even negative impact on the parameter correlations. However, these two designs are the only ones which target the enamine hydrogenation by increasing the CO/H_2 ratio to 1.8 and 8, respectively, and by adding water to the initial reaction mixture. While the first control decision directly impacts all reaction rates except for the enamine condensation by reducing the amount of the active catalyst in the system (see Eq. (1)), the addition of water causes a shift in the condensation equilibrium toward the substrates and, thus, limits the enamine hydrogenation rate. The interested reader is referred to Supplement H to answer the question if the information gained by the water addition compensate for the increased risk of phase separation during the experiment.

4.3. Results summary

Five experiments are designed to refine the parameter estimates for and extend the applicability of the 1-decene HAM model from Kortuz et al. [15] under a broad variety of (dynamic) operating conditions. All experiments are designed simultaneously by formulating the mbOED problem Eq. (E.6) and solving it using a multi-step initialization procedure to ensure feasible initial guesses and prevent the convergence toward local optima. The experiment designs with distinct concentration profiles result from the identification of optimal control parameters which lead to non-stoichiometric gas phase compositions and substrate ratios, the addition of water to the reaction mixture, variable experiment lengths and the utilization of nitrogen as an inert component to dilute the gas phase. The quantitative analysis of each experiment design's impact on the parameter uncertainties reveals the importance of designs 1 to 3 for the information gain on the decene isomerization, Hyfo and enamine condensation while designs 4 and 5 primarily focus on the enamine hydrogenation.

5. Model identification

This section summarizes the insights gained by the execution and analysis of the experiment designs from Section 4. In the first subsection, the extension of the reactor vessel model by a rigorous description of the gas phase is motivated to capture the limitations of the experiment setup. Subsequently, a structural modification of the catalyst pre-equilibrium is proposed to model the inhibiting effect of low H_2 concentrations on all catalyzed reactions. Finally, the parameter estimation procedure and a results subset are presented and discussed. Additional information on the experiments including an experiment overview (see table S2), the presentation of the experiment setup (see Fig. S2) and procedure as well as explanations of particular experiment choices can be found in Supplement A.

Table 2
Uncertainty ellipsoid volume $\det F^{-1}$, standard deviation σ and correlation matrix ρ based on the experiment designs from Fig. 4 and Table 1. The relative impact of each experiment design on these performance measures is identified by removing the contribution of design k from the FIM. The relative performance measures follow $\Delta \det F^{-1} = \det F \left(\det F_{\neg i}^{-1} - \det F^{-1}\right)^{-1}$, $\Delta\sigma_i = \left(\sigma_{i,\neg k} - \sigma_i\right)\sigma_i^{-1}$ and $\Delta|\rho_{i,j}| = |\rho_{i,j,\neg k}| - |\rho_{i,j}|$ with $i, j \in \{\text{Iso}, \text{Hyfo}, \text{Cond}, \text{HydEn}\}$ where the index $\square_{\neg k}$ denotes the removal of design k. Positive values negatively impact the respective performance measure. All results are based on the initial parameter guesses θ^0. The standard deviations and correlation coefficient matrix relate to the dimensionless activation energy B.

	$\det F^{-1}$ / 10^{-15}	σ / 10^{-2}		Correlation Matrix ρ			
				Iso	Hyfo	Cond	HydEn
	3.31	Iso	0.56	Iso	–	0.02	0.08	−0.01
		Hyfo	0.68	Hyfo	–	–	0.00	−0.29
		Cond	4.53	Cond	–	–	–	−0.14
		HydEn	3.58	HydEn	–	–	–	–
	$\Delta \det F^{-1}$ / %	$\Delta\sigma_i$ / %		Absolute Correlation Difference $\Delta\lvert\rho_{i,j}\rvert$			
Design 1	364.77	Iso	26.45	Iso	–	0.43	0.00	0.17
		Hyfo	59.08	Hyfo	–	–	0.26	0.12
		Cond	24.23	Cond	–	–	–	−0.11
		HydEn	4.88	HydEn	–	–	–	–
Design 2	321.33	Iso	2.35	Iso	–	0.02	0.02	0.01
		Hyfo	11.89	Hyfo	–	–	0.28	0.06
		Cond	87.09	Cond	–	–	–	0.11
		HydEn	2.62	HydEn	–	–	–	–
Design 3	433.03	Iso	119.34	Iso	–	0.46	0.09	0.23
		Hyfo	19.96	Hyfo	–	–	0.08	0.09
		Cond	1.18	Cond	–	–	–	−0.05
		HydEn	3.83	HydEn	–	–	–	–
Design 4	169.87	Iso	0.63	Iso	–	0.00	0.01	0.04
		Hyfo	3.58	Hyfo	–	–	0.02	0.00
		Cond	0.95	Cond	–	–	–	0.05
		HydEn	57.69	HydEn	–	–	–	–
Design 5	126.66	Iso	0.32	Iso	–	−0.01	0.01	0.01
		Hyfo	16.06	Hyfo	–	–	0.02	−0.12
		Cond	0.06	Cond	–	–	–	−0.03
		HydEn	25.00	HydEn	–	–	–	–

5.1. Rigorous gas phase model

When using the initial parameter guesses from tables S4 and S5 to simulate the experiments with the reactor vessel model from Eq. (B.3), significant deviations from the experimental concentration profiles are observable. As these deviations in the form of experimentally reduced reaction activities primarily occur for designs with gas phase compositions near the parameter bounds, depletion of one of the reaction gases seems plausible. To test this hypothesis, the detailed gas phase model in the form of the ordinary differential equation (ODE)

$$\frac{\mathrm{d}p_i}{\mathrm{d}t} = \Delta\dot{p}_i^{+} + \Delta\dot{p}_i^{-} + \frac{T}{V_{\text{Gas}}}\left(R\frac{\mathrm{d}n_i^{\text{Gas}}}{\mathrm{d}t} - \frac{p_i}{T}\frac{\mathrm{d}V_{\text{Gas}}}{\mathrm{d}t} + \frac{p_i V_{\text{Gas}}}{T^2}\frac{\mathrm{d}T}{\mathrm{d}t}\right), \tag{6a}$$

with the initial conditions

$$p_i\left(t^0\right) = p^0 y_i^0, \tag{6b}$$

for each gaseous species $i \in \mathcal{SPC}^{\text{Gas}}$ is introduced. While most terms originate from the assumption of ideal gas behavior, $\Delta\dot{p}_i^{+}$ and $\Delta\dot{p}_i^{-}$ describe the dosing and release of gas from the reactor vessel. The interested reader is referred to Supplement B.2 for the model derivation and an in-depth discussion on the modeling of each differential.

Concentration profile comparison. Fig. 5 provides a comparison of the concentration profiles with and without rigorous gas phase modeling for a subset of the experiments.

Without modification of the kinetic and thermodynamic parameter guesses, the grid columns contain the concentration profiles with (middle) and without (left) rigorous gas phase modeling as well as the pressure, temperature and gas phase composition profiles (right). When focusing first on experiments 48a_D2 and 50a_D4, the concentration profiles of substrates and final products are replicated accurately without any major differences in prediction quality between both gas phase formulations. In contrast, simulating experiment 53c_D3 using both implementations yields significant differences in terms of overall system reactivity. The improved accuracy of the rigorous gas phase formulation lies in the depiction of H_2 depletion in the first 20 min. Favored by the low partial pressure of H_2 in design 3, the imbalance in the consumed and supplied gas ratio leads to this rapid depletion of the gaseous substrate despite the periodic purging of the gas phase (identifiable by the high volatility in the pressure control of experiment 53_D3 in Fig. 5). It is important to note that the low vapor pressure of DEA impedes a more aggressive purging strategy and, therefore, does not represent an alternative to the accurate modeling of the gas phase.

Gas phase model limitations. While the rigorous gas phase modeling is able to improve the replication of experiment 53c_D3, it is not able to remedy the underestimation of decene isomerization in experiment 49a_D1. When comparing the latter experiment to its design simulation in Fig. 4(a), the match between the experimental and designed concentration profiles is surprising due to the qualitatively different results from the simulative replication of the operating conditions (compare the simulated concentration profiles in Fig. 4(a) with the top row in Fig. 5). Besides the adjustment of the burette's H_2 content to 80% in contrast to the designed 92%, no alterations to the operating conditions are performed. While the H_2 content increases in the first minutes, a steeper increase would be required to match the designed gas phase ratio. However, this system behavior does not seem to be likely as the gas phase dynamics in all other experiments enable accurate replications of the concentration profiles. Hence, inaccurate reaction kinetics can be expected to cause the mismatch between the experimental and simulated profiles. More precisely, the catalyst pre-equilibrium in Eq. (1) appears to be more sensitive to low CO concentrations (see the first 10 min in experiment 46a_D1 where the pressure ramp is located). To correct this behavior, the exponent of the CO concentration

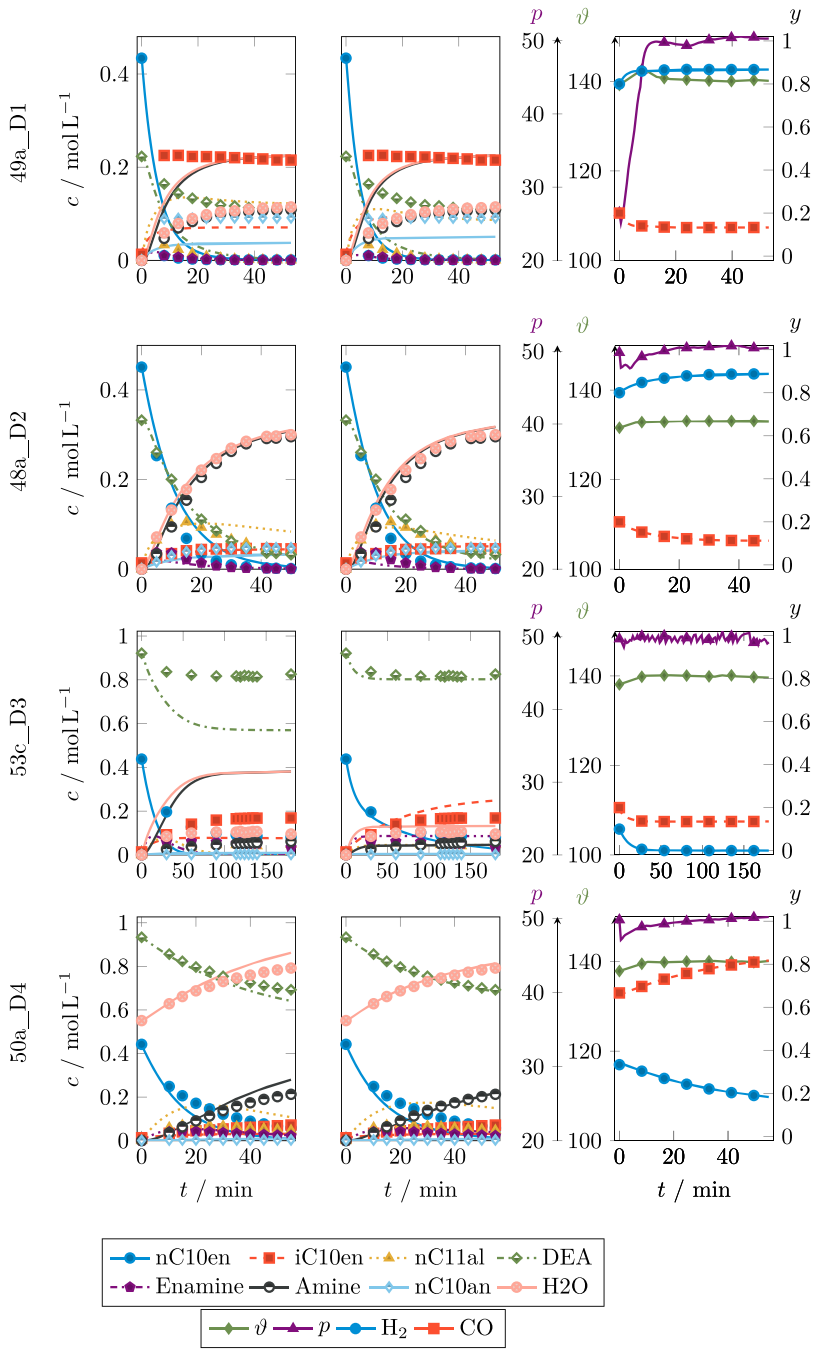

Fig. 5. Comparison of predicted concentration profiles of selected experiments using the parameters from tables S4 and S5. Concentration profiles visualized via continuous lines represent the simulation results while marks are used for the experimental data. Left: Ideal control of the gas phase composition. Middle: Rigorous gas phase model from Eq. (B.7). Right: Experimental control profiles and predicted gas phase composition using the rigorous gas phase model. Here, marks do not represent experimental measurements and are solely used for visualization purposes.

in the inhibition term of Eq. (1) is considered as an additional degree of freedom during parameter estimation. A similar formulation was already presented by Jörke et al. [25] in the more rigorous description of the catalyst equilibrium.

5.2. Modified catalyst pre-equilibrium

Further inspection of the concentration profiles in 53c_D3 and 53b_D3 (see Fig. S3 in Supplement A) reveals additional optimization potential w.r.t. the prediction of the decene isomerization. In both experiments, the isomer concentration reaches the steady-state significantly earlier when compared to the simulations. Interestingly, the loss of the reaction activity coincides with the depletion of the H_2 in the gas phase and matches earlier observations by Kiedorf et al. [16] who encountered the formation of inactive catalyst dimers in the absence of H_2. Therefore, an inhibition term is added to the catalyst pre-equilibrium for the case of H_2 absence

$$c_{\mathrm{cat}} = \frac{c_{\Sigma\mathrm{cat}}}{1 + K_{\mathrm{cat,CO}} c_{\mathrm{CO}}^{a_{\mathrm{cat,CO}}} + K_{\mathrm{cat,H_2}} c_{\mathrm{H_2}}^{a_{\mathrm{cat,H_2}}}}, \tag{7}$$

Please note that $a_{\mathrm{cat,H_2}}$ is expected to be negative under these circumstances and, therefore, follows the formulations from Kiedorf et al. [16] and Hentschel et al. [17]. To prevent numeric issues in edge cases, a heuristic formulation is employed in which the H_2 concentration is used

Table 3
Kinetic parameters estimates for the HAM of 1-decene. All parameters are identifiable according to the local parameter subset selection approach from Barz et al. [21] with the numerical threshold from Jörke et al. [13]. The presented uncertainties represent one standard deviation.

i	A_i / −	B_i / −
Iso	4.9207 ± 0.0005	51.0316 ± 0.0053
Hyfo	17.5367 ± 0.0012	26.0423 ± 0.0019
Cond	−1.5277 ± 0.0005	12.6183 ± 0.0035
HydEn	15.3488 ± 0.2172	26.1398 ± 2.3242
HydDec	9.8808 ± 0.0007	33.1396 ± 0.0019

$K_{cat,CO}$ / −	82 305.0902	± 2.3631
$a_{cat,CO}$ / −	1.6017	± 0.0002
K_{cat,H_2} / −	0.035 00	± 0.000 01
a_{cat,H_2} / −	−1.2669	± 0.0002
[a] $K_{Hyfo,I}$ / L mol^{-1}	92.1	
[a] $K_{Hyfo,II}$ / L^2 mol^{-2}	1063.6	
[b] K_{Iso}^{eq} / −	39.0	
[a] $\Delta G_{r,Cond}$ / J mol^{-1}	4000	
[a] K_{HydEn} / L mol^{-1}	6.49	
[a] K_{HydDec} / L mol^{-1}	10.2	

[a]Fixed at initial guess. See table S5 for the literature reference.
[b]Estimated from preliminary experiments.

directly instead of relying on the gas concentration ratio from Kiedorf et al. [16]. Under these circumstances, a_{cat,H_2} is expected to be negative. Without the possibility to measure the catalyst species concentration via operando Fourier transform infrared spectroscopy (FTIR) due to the corrosive effect of DEA, the inhibition constants and exponents for the CO and H_2 concentrations in Eq. (7) need to be estimated from the kinetic experiment data.

5.3. Parameter identification

The reactor vessel model and catalyst pre-equilibrium alterations from Sections 5.1 and 5.2 allow the parameter identification for the 1-decene HAM.

Parameter selection. While the number of parameters during mbOED needs to be restricted to reduce the computational load, all dimensionless kinetic parameters A_j and B_j for all $j \in \mathcal{RCT}^{HAM}$ can be considered during parameter estimation. Additionally, the inhibition constants $K_{cat,i}$ and exponents $a_{cat,i}$ for $i \in \mathcal{SPC}^{Gas}$ in the catalyst pre-equilibrium are added which leads to a total of 14 uncertain parameters. All of the remaining inhibition constants and the isomerization equilibrium constant are fixed either based on literature data or by using preliminary measurements to improve the condition number of the FIM and to ensure identifiability.

Estimation results. Parameter estimation is performed using a general least-squares (LSQ) formulation (see table S10 for the measurement uncertainty) in a multi-start algorithm with parameter scaling and local parameter subset selection [21]. The final parameter estimates are summarized in Table 3. All of the experiments which are used during the parameter estimation are marked in table S2. Detailed information on the parameter identification algorithm can be found in Algorithm 1 in Supplement F.

The low standard deviation of the kinetic and inhibition parameters align with the identifiability of all parameters according to the parameter subset selection in Algorithm 1. From the kinetic parameters, only the enamine hydrogenation exhibits an increased parameter uncertainty for both kinetic parameters A_{HydEn} and B_{HydEn}. This is expected as the reaction is fast and only limited information can be extracted from the experiments (see Supplement H for the positive effect of water dosing for the identifiability of the enamine hydrogenation). Comparing the estimation results with the initial guesses (see table S4), the dimensionless parameter A_j with $j \in \mathcal{RCT}^{HAM}$ remain nearly unchanged. This supports the prior assumption of high quality parameter guesses in conjunction with a suitable preliminary kinetic model structure. More pronounced adjustments occur in terms of the dimensionless activation energy B_j which increases by approximately 13 kJ mol^{-1} and 35 kJ mol^{-1} in non-dimensionless form for the Hyfo and isomerization, respectively. For the isomerization, this leads to an activation energy of 158 kJ mol^{-1} which is significantly different from its initial guess but still lies in the same order of magnitude. Alongside this increase in isomerization activation energy, the CO inhibition constant in the catalyst pre-equilibrium rises by one order of magnitude to balance the activation energy adjustment and the elevated CO concentration exponent which aligns with literature data (1.6017 instead of 1.7406 for the investigation of the Hyfo by Jörke et al. [25]).

Prediction quality. Exemplified by the experiment selection in Fig. 6, the combination of a rigorous gas phase model, a refined description of the catalyst pre-equilibrium and improved parameter estimates yields a drastically increased quality of the simulated concentration profiles.

In contrast to the predictions prior to the parameter estimation, the decene isomerization is now depicted accurately in experiment 49a_D1, owing to the adjusted CO inhibition of the active catalyst species alongside the elevated isomerization activation energy. This also benefits the simulation of the co-substrate consumption, aldehyde formation, decene hydrogenation as well as amine and water production even though minor deviations still occur under these operating conditions. It can be assumed that these overestimations of the reaction activity can be attributed to the approximated catalyst inhibition model which requires additional attention to describe the catalyst activity under (selective) gas phase species depletion.

In experiment 48a_D2, changes due to the improved catalyst equilibrium and parameter refinement are scarce because of the near nominal operating conditions and the abundance of data available from previous experiments for these operating conditions (see table S2). Nevertheless, the accuracy of the aldehyde concentration profile can be increased at the expense of a slightly overestimated decane and underestimated enamine formation.

While the reduced enamine condensation activity leads to a minor decrease in prediction quality for the previous experiment, it significantly improves the enamine concentration profile in experiment 54a_D3. Being the only non-catalyzed reaction in the reaction network, the lower enamine concentration is caused indirectly by the reactivity decreasing effect of the H_2-induced decrease in catalyst activity. The direct influence of the H_2 depletion is apparent for the isomerization reaction for which the prediction is able to fit the experimental observations. Simultaneously, the additional availability of 1-decene leads to a better approximation of the amine concentration.

Lastly, experiment 53a_D3 represents one of the best examples for the decremental effect of H_2 absence on the systems reactivity. If the catalyst pre-equilibrium would be unaffected by the H_2 content in the gas phase, the decene isomerization should not encounter any restrictions. However, as the reduced catalyst activity significantly improves the prediction of the isomer concentration and substrate consumption, the conclusions from the investigation of the catalyst pre-equilibrium by Jörke et al. [25], Kiedorf et al. [16] seem to be directly transferable to the HAM in a MeOH/nC12an TMS.

For the interested reader, Supplement F contains the predictions of all experiment designs from table S2 in the form of detailed concentration profile comparisons (see Fig. S7) and parity plots (see Fig. S6).

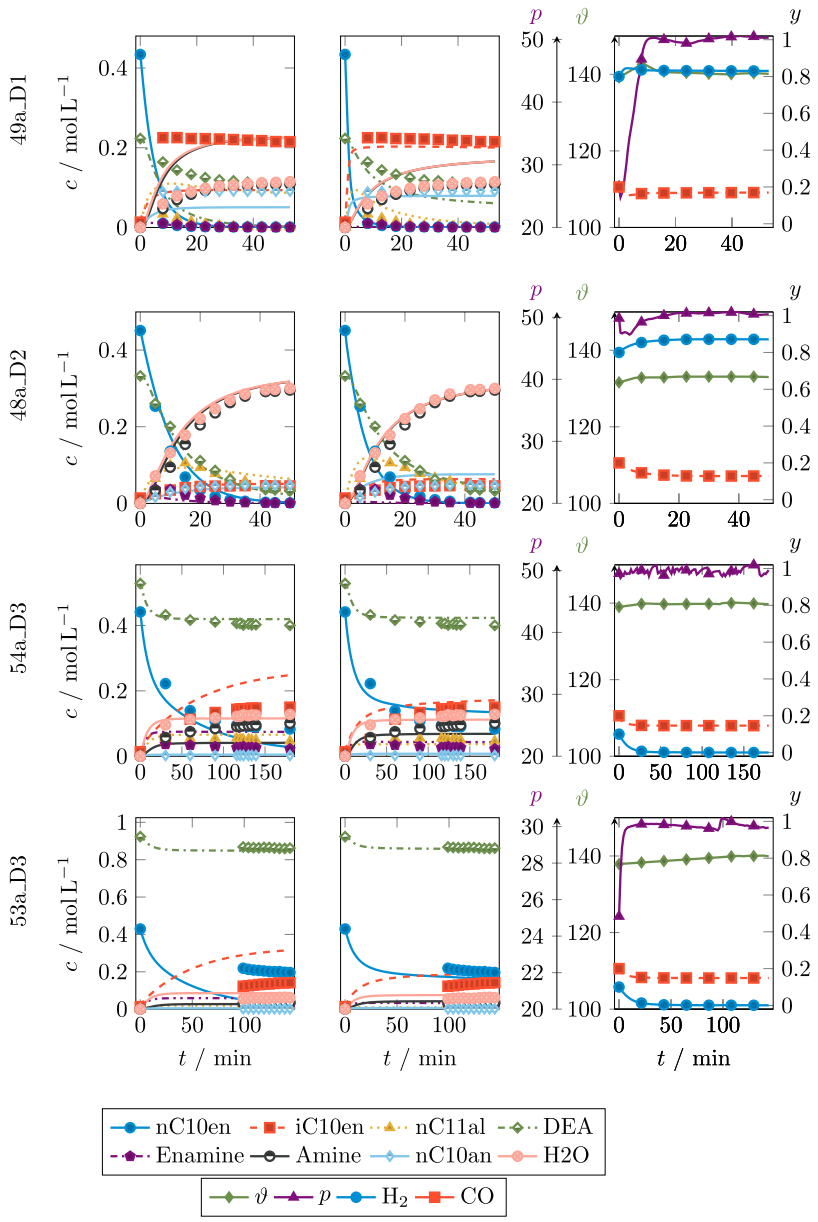

Fig. 6. Comparison of predicted (lines) and experimental concentration profiles (marks) of selected experiments. Left: Reactor vessel model from Eq. (B.3) with rigorous gas phase description from Eq. (B.7) and initial parameter guesses from table S4. Middle: Reactor vessel model form Eq. (B.3) with rigorous gas phase description from Eq. (B.7) and estimated parameter values from Table 3. Right: Experimental control profiles and predicted gas phase composition using the rigorous gas phase model with the estimated parameter values from Table 3. Here, marks do not represent experimental measurements and are solely used for visualization purposes. A comparison between all predicted and experimental concentration profiles using the parameters from Table 3 and the rigorous gas model can be found in Fig. S7 in Supplement F.

Kinetic model limitations. Despite the significant improvements in the prediction quality, the new kinetic model is not able to replicate the concentration profiles under all considered operating conditions. These shortcomings can be exemplified using the repetition experiments 55a_D3 and 55b_D3 in Fig. 7.

In both cases, low H_2 partial pressures lead to a slow depletion of the gaseous species over the experiment time. While the inhibition of the catalyst due to low H_2 concentrations should be accounted for by the addition of a dedicated inhibition term in the catalyst pre-equilibrium, the concentration profiles clearly indicate that the reaction activity is significantly overestimated. After 20 min, the experimental substrate consumption and product formation stagnate even though H_2 is still available with approximately 6 bar. This indicates the necessity for a more rigorous formulation of the catalyst pre-equilibrium which is able to incorporate threshold concentrations after which the catalyst dimer formation accelerates.

5.4. Results summary

Based on experimental observations, the initial reactor vessel model is extended by a rigorous gas phase model to account for the difference in gas phase concentration ratio and gas consumption by the reaction system under edge case operating conditions. Furthermore, an inhibition term for the catalyst activity in the absence of H_2 in the liquid phase is introduced to match the experimental results w.r.t. the isomerization activity. In addition to these structural changes, a parameter estimation is performed using a multi-start procedure with integrated identifiability detection. All kinetic parameter A_j and B_j with $j \in \mathcal{RCT}^{\mathrm{HAM}}$ as well as the inhibition constants and exponents for the CO and H_2 inhibition in the catalyst pre-equilibrium are considered during parameter estimation. After identifying all parameters with high accuracy, the comparison of simulated and experimental concentration profiles yields a satisfactory match not only for nominal operating

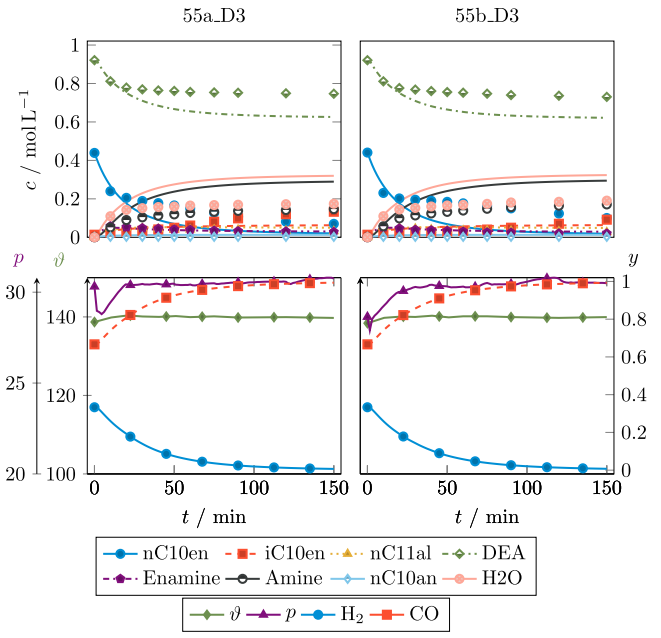

Fig. 7. Comparison of the predicted and experimental concentration profiles of experiment 55a_D3 and 55b_D3 (see table S2). The predicted concentration profiles are calculated using the estimated parameter values from Table 3. Concentration profiles visualized via continuous lines represent the simulation results while marks are used for the experimental data. Marks in the control profile plots do not represent experimental measurements and are solely used for visualization purposes.

conditions but also for edge cases with abundant or limited CO or H_2 supply.

6. Summary and conclusions

Summary. The homogeneously rhodium-catalyzed tandem hydroaminomethylation (HAM) of 1-decene in a MeOH/nC12an TMS is investigated to refine and improve the prediction quality of the kinetic model from Kortuz et al. [15]. MbOED is utilized to simultaneously design five, optimally complementing experiments to identify kinetic reaction parameters. Besides frequently used control parameters such as temperature, pressure, gas phase composition and the substrate to co-substrate ratio, the experiment time, optimal measurement points as well as the initial water amount are utilized as DoFs to achieve the D-optimal minimum of parameter uncertainty. The feasibility and practicability of each experiment design is ensured by incorporating constraints replicating technical and human limitations. The risk of phase separation because of water accumulation from the enamine condensation during the reaction is confronted by incorporating monophasic constraints using phase equilibrium calculations. The phase equilibrium calculations utilize a custom-designed PC-SAFT-based activity coefficient ANN.

Including repetitions and adjusted experiment designs, a total of 12 experiments were performed relying on four optimal designs and used for the model adjustment. Besides the introduction of a rigorous gas phase formulation for the reactor vessel model, the catalyst pre-equilibrium is refined to incorporate the catalyst dimer formation under low H_2 concentrations. Additionally, a multi-start parameter estimation with parameter subset selection yields identifiable and accurate kinetic and inhibition parameters which significantly improve the model's prediction quality under edge cases. Overall, both substrates, the product amine as well as the water accumulation is predicted with high precision in all studied scenarios so that the initially motivated investigation and description of the water influence on the reaction system can be considered successful.

Conclusions. Especially non-standard operating conditions, under which either H_2 depletion or low CO partial pressures may occur, cannot be predicted sufficiently by the HAM model from Kortuz et al. [15]. The application of mbOED is able to yield experiment designs which disclose these weaknesses and facilitate structural and parametric refinements. The combination of a reactor vessel model including a detailed gas phase description in conjunction with improved reaction kinetics is able to replicate the investigated edge cases while maintaining the simulation accuracy under nominal operating conditions.

Despite the significant improvements of the kinetic model, a small subset of operating scenarios exhibit higher deviation from the experimental data. Besides the replication of concentration profiles of intermediate products such as 1-undecanal and the enamine, the simulation of experiments with a prolonged H_2 depletion period is challenging. While the latter case suggests a closer look at the catalyst pre-equilibrium model, an improved estimation of intermediate species' concentration profiles is only possible by additional experimental data. However, even in the case of experiments which target the inner edges of the reaction network, substantially higher accuracy of the predictions, especially of the enamine, cannot be expected due to the missing calibration standards. In general, missing calibration standards represents one of the most important shortcomings in today's reaction analytics and will become even more challenging for future investigations of long-chain aldehydes, enamines and other products based on renewable feedstock.

Declaration of competing interest

The authors declare the following financial interests/personal relationships which may be considered as potential competing interests: Kai Sundmacher reports financial support was provided by German Research Foundation. Kai Sundmacher reports financial support was provided by Ministry for Science, Energy, Climate Protection and the Environment of the State of Saxony-Anhalt.

Data availability

Data will be made available on request.

Acknowledgments

Gefördert durch die Deutsche Forschungsgemeinschaft (DFG) - TRR 63 "Integrierte chemische Prozesse in flüssigen Mehrphasensystemen" (Teilprojekt B1) - 56091768. Funded by the Deutsche Forschungsgemeinschaft (DFG, German Research Foundation) - TRR 63 "Integrated Chemical Processes in Liquid Multiphase Systems" (subproject B1) - 56091768. This work is also part of the research initiative "SmartProSys: Intelligent Process Systems for the Sustainable Production of Chemicals" funded by the Ministry for Science, Energy, Climate Protection and the Environment of the State of Saxony-Anhalt. The author Karsten H. G. Rätze is also affiliated with the "International Max Planck Research School (IMPRS) for Advanced Methods in Process and Systems Engineering (Magdeburg)".

Appendix A. Supplementary data

Supplementary material related to this article can be found online at https://doi.org/10.1016/j.cej.2023.143713.

References

[1] P. Roose, K. Eller, E. Henkes, R. Rossbacher, H. Höke, Amines, aliphatic, in: Wiley-VCH Verlag GmbH & Co. KGaA (Ed.), Ullmann's Encyclopedia of Industrial Chemistry, Wiley-VCH Verlag GmbH & Co. KGaA, Weinheim, Germany, 2015, pp. 1–55, http://dx.doi.org/10.1002/14356007.a02_001.pub2.

[2] T.A. Faßbach, F.O. Sommer, A.J. Vorholt, Hydroaminomethylation in aqueous solvent systems - An efficient pathway to highly functionalized amines, Adv. Synth. Catal. 360 (2018) 1473–1482, http://dx.doi.org/10.1002/adsc.201701463.

[3] M. Beller, J. Seayad, A. Tillack, H. Jiao, Catalytic Markovnikov and anti-Markovnikov Functionalization of alkenes and alkynes: Recent developments and trends, Angew. Chem. Int. Ed. 43 (2004) 3368–3398, http://dx.doi.org/10.1002/anie.200300616.

[4] M. Kraume, S. Enders, A. Drews, S. Schomäcker, K. Sundmacher, Integrated Chemical Processes in Liquid Multiphase Systems: from Chemical Reaction To Process Design and Operation, De Gruyter, 2022, http://dx.doi.org/10.1515/9783110709858.

[5] M. Ahmed, A.M. Seayad, R. Jackstell, M. Beller, Amines made easily: A highly selective hydroaminomethylation of olefins, J. Am. Chem. Soc. 125 (2003) 10311–10318, http://dx.doi.org/10.1021/ja030143w.

[6] W. Kortuz, S. Kirschtowski, A. Seidel-Morgenstern, C. Hamel, Kinetics of the rhodium-catalyzed hydroaminomethylation of 1-decene in a thermomorphic solvent system, Chem. Ing. Tech. 94 (2022) 760–765, http://dx.doi.org/10.1002/cite.202100180.

[7] S. Kirschtowski, F. Jameel, M. Stein, A. Seidel-Morgenstern, C. Hamel, Kinetics of the reductive amination of 1-undecanal in thermomorphic multicomponent system, Chem. Eng. Sci. 230 (2020) 116187, http://dx.doi.org/10.1016/j.ces.2020.116187.

[8] T.A. Faßbach, T. Gaide, M. Terhorst, A. Behr, A.J. Vorholt, Renewable surfactants through the hydroaminomethylation of terpenes, ChemCatChem 9 (2017) 1359–1362, http://dx.doi.org/10.1002/cctc.201700097.

[9] K. McBride, N.M. Kaiser, K. Sundmacher, Integrated reaction–extraction process for the hydroformylation of long-chain alkenes with a homogeneous catalyst, Comput. Chem. Eng. 105 (2017) 212–223, http://dx.doi.org/10.1016/j.compchemeng.2016.11.019.

[10] D.E. Bergbreiter, Y.S. Liu, P.L. Osburn, Thermomorphic rhodium(I) and palladium(0) catalysts, J. Am. Chem. Soc. 120 (1998) 4250–4251, http://dx.doi.org/10.1021/ja980136l.

[11] J. Bianga, K.U. Künnemann, L. Goclik, L. Schurm, D. Vogt, T. Seidensticker, Tandem catalytic amine synthesis from alkenes in continuous flow enabled by integrated catalyst recycling, ACS Catal. 10 (2020) 6463–6472, http://dx.doi.org/10.1021/acscatal.0c01465.

[12] M. Illner, A. Weber, L. Hohl, M. Petzold, N. Afraz, K. Hecht, L. Böhm, A. Drews, J.U. Repke, R. Schomäcker, Microemulsion systems, in: M. Kraume, S. Enders, A. Drews, R. Schomäcker, S. Engell, K. Sundmacher (Eds.), Integrated Chemical Processes in Liquid Multiphase Systems - from Chemical Reaction To Process Design, De Gruyter, 2022, http://dx.doi.org/10.1515/9783110709858.

[13] A. Jörke, T. Gaide, A. Behr, A. Vorholt, A. Seidel-Morgenstern, C. Hamel, Hydroformylation and tandem isomerization–hydroformylation of n-decenes using a rhodium-BiPhePhos catalyst: Kinetic modeling, reaction network analysis and optimal reaction control, Chem. Eng. J. 313 (2017) 382–397, http://dx.doi.org/10.1016/j.cej.2016.12.070.

[14] W. Kortuz, Kopplung von hydroformylierung und reduktiver aminierung in der tandemreaktion hydroaminomethylierung -kinetische modellbildung und beschreibung, Master's thesis, Otto-von-Guericke-Universität. Magdeburg, 2020.

[15] W. Kortuz, S. Kirschtowski, A. Seidel-Morgenstern, C. Hamel, Mechanistic kinetic modeling of the rhodium-catalyzed tandem hydroaminomethylation of 1-decene in a thermomorphic solvent system, Catal. Commun. 177 (2023) 106633, http://dx.doi.org/10.1016/j.catcom.2023.106633.

[16] G. Kiedorf, D. Hoang, A. Müller, A. Jörke, J. Markert, H. Arellano-Garcia, A. Seidel-Morgenstern, C. Hamel, Kinetics of 1-dodecene hydroformylation in a thermomorphic solvent system using a rhodium-biphephos catalyst, Chem. Eng. Sci. 115 (2014) 31–48, http://dx.doi.org/10.1016/j.ces.2013.06.027.

[17] B. Hentschel, G. Kiedorf, M. Gerlach, C. Hamel, A. Seidel-Morgenstern, H. Freund, K. Sundmacher, Model-based identification and experimental validation of the optimal reaction route for the hydroformylation of 1-dodecene, Ind. Eng. Chem. Res. 54 (2015) 1755–1765, http://dx.doi.org/10.1021/ie504388t.

[18] A. Jörke, A. Seidel-Morgenstern, C. Hamel, Isomerization of 1-decene: Estimation of thermodynamic properties, equilibrium composition calculation and experimental validation using a Rh-BIPHEPHOS catalyst, Chem. Eng. J. 260 (2015a) 513–523, http://dx.doi.org/10.1016/j.cej.2014.09.015.

[19] M. Schwaab, J.C. Pinto, Optimum reference temperature for reparameterization of the Arrhenius equation. Part 1: Problems involving one kinetic constant, Chem. Eng. Sci. 62 (2007) 2750–2764, http://dx.doi.org/10.1016/j.ces.2007.02.020.

[20] F. Galvanin, S. Macchietto, F. Bezzo, Model-based design of parallel experiments, Ind. Eng. Chem. Res. 46 (2007) 871–882, http://dx.doi.org/10.1021/ie0611406.

[21] T. Barz, D.C. López Cárdenas, H. Arellano-Garcia, G. Wozny, Experimental evaluation of an approach to online redesign of experiments for parameter determination, AIChE J. 59 (2013) 1981–1995, http://dx.doi.org/10.1002/aic.13957.

[22] S. Schlüter, K.U. Künnemann, M. Freis, T. Roth, D. Vogt, J.M. Dreimann, M. Skiborowski, Continuous co-product separation by organic solvent nanofiltration for the hydroaminomethylation in a thermomorphic multiphase system, Chem. Eng. J. 409 (2021) 128219, http://dx.doi.org/10.1016/j.cej.2020.128219.

[23] F. Huxoll, S. Schlüter, R. Budde, M. Skiborowski, M. Petzold, L. Böhm, M. Kraume, G. Sadowski, Phase equilibria for the hydroaminomethylation of 1-decene, J. Chem. Eng. Data 66 (2021) 4484–4495, http://dx.doi.org/10.1021/acs.jced.1c00561.

[24] A. Zinser, L. Rihko-Struckmann, K. Sundmacher, Dynamic method for computation of chemical and phase equilibria, Comput. Chem. Eng. 89 (2016) 1–10, http://dx.doi.org/10.1016/j.compchemeng.2016.02.014.

[25] A. Jörke, S. Triemer, A. Seidel-Morgenstern, C. Hamel, Kinetic investigation exploiting local parameter subset selection: isomerization of 1-Decene using a Rh-Biphephos catalyst, Chem. Ing. Tech. 87 (2015b) 713–725, http://dx.doi.org/10.1002/cite.201400148.

Glossary

0: initial value
$\emptyset$: empty set
A: dimensionless kinetic constant
$\mathcal{A}$: surface area
B: dimensionless kinetic constant
E_A: activation energy
$\mathcal{EXP}$: set of experiments
F: Fisher information matrix
FE: finite element
$\mathcal{GAS}$: set of gaseous chemical species
Gas: gaseous
ΔG_r: Gibbs enthalpy of reaction
H: Henry coefficient
Θ: set of uncertain parameters
K^{eq}, K: equilibrium constant, inhibition coefficient
L: lower bound value
Lig: ligand
Liq: liquid
$\tilde{M}$: molar mass
$\mathbb{N}_+$: positive natural numbers excluding zero
$\mathcal{P}$: time-independent control set
R: universal gas constant
$\mathcal{RCT}^{\text{HAM}}$: set of reactions in the hydroaminomethylation
$\mathbb{R}$: real numbers
$\mathcal{SPC}$: set of chemical species
$\mathcal{SPC}^{\text{ANN}}$: set of chemical species in ANN
$\mathcal{SPC}^{\text{Gas}}$: set of gaseous chemical species
$\mathcal{SPC}^{y}$: set of measured chemical species
T: temperature
U: upper bound value
$\mathcal{U}$: time-dependent control set
V: volume-based
V: volume
$\mathcal{X}$: states set
a: activity
c: molar concentration
cat: active catalyst
Σcat: catalyst precursor
c: constants
eff: effective
eq: equilibrium
exp: experiment
f: final value
f: RHS of an ODE system
g: AE system, path equality constraints
g^{f}: terminal inequality constraints
h: path equality constraints
h^{f}: terminal equality constraints
h_{FE}: finite element width
j: dosing / diffusion flow
k: kinetic rate factor
k_0: collision factor
m: mass-based
m: mass
n: molar-based
n, n: molar amount, number of
p: pressure
p: time-independent decision variables
prior: prior / previous information
prod: product
r: reaction rate

red: reduced
ref: reference
s: slope
sat: saturation
set: setpoint
sim: simulation
sp: sampling point
sub: substrate
t: time
u: inputs
u: time-dependent decision variables
w: mass fraction
x: molar fraction in the liquid phase
χ: state variables
y: molar fraction in the gaseous phase
y: measured variables / outputs
Σ: variance-covariance matrix
Π: set comprising all phases
$\mathcal{T}$: time domain
β: mass transfer coefficient
γ: activity coefficient, colinearity measure
ϵ: deviation between measurement and prediction
ε: machine precision, small number
η: measurement data
θ: uncertain parameters
ϑ: temperature
κ: bleeding of species to secondary phases, invertibility measure
$-$: removal
ν: stoichiometric matrix
ρ: density, correlation matrix
$+$: dosing / addition
σ: standard deviation
ϕ: objective function, ratio
ω: sampling decisions
$\square$: flow
$\hat{\square}$: estimated value, expectation value
$\square_{\neg\square}$: without
$\tilde{\square}$: normalized, scaled, transformed variable
$\square^*$: optimal solution, true value
amine: n,n-diethylundecylamine (hydrogenated)
ANN: artificial neural network
C10an: n-decane
CO: carbon monoxide
Cond: (enamine) condensation reaction of the hydroaminomethylation
CPH: chemical properties handbook
DAE: differential algebraic equation
DEA: diethylamine
DIPPR: design institute for physical properties
DMF: n,n-dimethylformamide
DoF: degree of freedom
DOP: dynamic optimization program
enamine: n,n-diethylundecylamine
EoS: equation of state
FIM: Fisher information matrix
FTIR: Fourier transform infrared spectroscopy
GC: group contribution
H_2: hydrogen
H_2O: water
HAM: hydroaminomethylation
HydDec: 1-decene hydrogenation in the hydroaminomethylation
HydEn: enamine hydrogenation in the hydroaminomethylation and reductive amination
Hyfo: hydroformylation
iC10en: decene isomers
iC11al: undecanal isomers
IPOPT: interior point optimizer
Iso: olefin isomerization reaction in the hydroaminomethylation
LLE: liquid-liquid equilibrium
LSQ: least-squares
mbOED: model-based optimal experimental design
MeOH: methanol
MIDOP: mixed-integer dynamic optimization program
modUNIFAC: modified UNIFAC(Dortmund)
N_2: nitrogen
nC10en: 1-decene
nC11al: 1-undecanal
nC12an: n-dodecane
NLP: non-linear optimization program
ODE: ordinary differential equation
PC-SAFT: perturbed-chain statistical associating fluid theory
RA: reductive amination
Rh(acac)(COD): (acetylacetonato)(1,5-cyclooctadiene)rhodium(I)
RHS: right hand side
SulfoXantphos: 4,5-bis(diphenylphosphino)-9,9-dimethyl-2,7-disulfoxanthene disodium salt
TMS: thermomorphic multiphase system
w.r.t.: with respect to